DEM simulations of the small strain stiffness of granular soils: effect of stress ratio

Xiaoqiang Gu · Jun Yang · Maosong Huang

Abstract DEM (discrete element method) simulations are carried out to evaluate the small strain stiffness (i.e. Young's modulus and shear modulus) of a granular random packing with focus on the effect of stress ratio (SR). The results show that the Young's modulus in a given direction generally depends on the stress component in that direction. The Young's modulus normalized by the related stress component remains nearly constant when SR is less than a threshold value SR_{th}. When SR is larger than SR_{th}, the normalized Young's modulus decreases, particularly in the minor principle stress direction. Moreover, the Young's modulus during unloading is always smaller than the one during loading at the same stress state, which indicates that the microstructure of the specimen has been modified by the historical shearing process. The shear modulus mainly depends on the mean effective stress and shows similar evolution trend as the Young's modulus. This study finds that the macroscopic stiffness of the specimen is closely related to the evolutions of particle contact number and contact force during shearing. When SR is less than SR_{th}, the specimen only adjusts the distribution of contact forces to resist the external load, without any apparent change of contact number. When SR is larger than SR_{th}, however, the specimen has to adjust both contact number and contact forces to resist the external load. The study also illustrates that there is a good relationship between the macroscopic stiffness anisotropy and fabric anisotropy, and therefore the stiffness anisotropy may be used as an indicator of fabric anisotropy.

Keywords Discrete element · Small strain stiffness · Young's modulus · Shear modulus · Stress ratio · Anisotropy

X. Gu (✉) · M. Huang
Department of Geotechnical Engineering, Tongji University,
Shanghai 200092, China
e-mail: gxq1981@gmail.com

M. Huang
e-mail: mshuang@tongji.edu.cn

X. Gu · M. Huang
Key Laboratory of Geotechnical and Underground
Engineering of the Ministry of Education, Tongji University,
Shanghai 200092, China

J. Yang
Department of Civil Engineering, The University of Hong Kong,
Pokfulam, Hong Kong, China
e-mail: junyang@hku.hk

Abbreviations

DEM	Discrete element method
SR	Stress ratio
CN	Coordination number
NCF	Normal contact force
TC	Triaxial compression
TE	Triaxial extension
IC	Isotropic compression
AC	Axial compression
AE	Axial extension

1 Introduction

It is well known that soil behavior is generally nonlinear and plastic in nature. However, at strain level below 0.001 %, the response of soils is usually assumed to be linear and elastic, and the corresponding stiffness are referred to as small strain stiffness (e.g. shear modulus G_0 and Young's modulus E_0). The small strain stiffness plays important roles in many geotechnical problems, such as machine foundations,

earthquake ground response analysis and liquefaction potential evaluation [1–3].

At early stages, the small strain stiffness is usually measured by resonant column tests at isotropic stress states. The measurements have convincingly showed that the G_0 or E_0 for a given granular soil mainly depends on its void ratio e (or soil density) and effective stress σ'_0, and can be expressed by the following general form [4]

$$G_0 (\text{or } E_0) = A F(e) \left(\frac{\sigma'_0}{p_a} \right)^n \qquad (1)$$

where A is a constant reflecting soil type, grain properties and fabric, p_a is a reference stress, n is the stress exponent reflecting the effect of effective stress, and $F(e)$ is a void ratio function reflecting the effect of soil density.

However, the actual stress state in the field is always anisotropic and therefore laboratory tests are also performed at anisotropic stress states to investigate the effect of individual stress component or the stress ratio (SR) on the G_0 [5–11]. Hardin and Black [5] showed that Eq. (1) worked for the anisotropic stress states when σ'_0 was replaced by the mean effective stress $(\sigma'_1 + \sigma'_2 + \sigma'_3)/3$, which indicated that the shear stress or the SR had ignorable effect on the G_0. On the other hand, Tatsuoka et al. [6] reported that the SR had effect on the G_0 and the effect was more significant in triaxial extension (TE) than in triaxial compression (TC). Roesler [7] and Knox et al. [8] indicated that the G_0 depended on the stress components in the wave propagation direction σ'_a and in the particle motion direction σ'_p, but was independent of the out-of-plane stress component. Therefore, the average stress $\sigma'_m = (\sigma'_a + \sigma'_p)/2$ should be used in Eq. (1) instead of σ'_0 and the G_0 is usually denoted as G_{ap}. Yu and Richart [9] found that SR had effect on the G_0 and the degree depended on the shear strength of the soil. They also found that the G_0 value might decrease after a shear stress history, which indicated that the microstructure of the specimen was modified by the historical shear stress.

Contrast to the G_0, it has been found that the small strain Young's modulus in a given direction E_i generally depends only on the stress component in that direction σ'_i [11–15]. Hoque and Tatsuoka [15] showed that there was a threshold stress ratio SR_{th} (i.e. 2.0) for a dense Toyoura sand specimen ($e = 0.65$) during TC, below which the normalized Young's modulus $E_i/(\sigma'_i)^{ni}$ was nearly constant and beyond which it decreased with increasing SR, as shown in Fig. 1. Toyoura sand is a clean and uniform quartz sand with sub-angular particle shape. As seen in Fig. 1, it worth noting that the degree of decrease is more significant in the major principle stress direction. The authors attributed the decrease of normalized Young's modulus to the damage of initial fabric especially in the major principle stress direction. However, Ezaoui and Di Benedetto [11] investigated the anisotropic elastic behavior of uniform and sub-angular Hostun sand by triaxial tests,
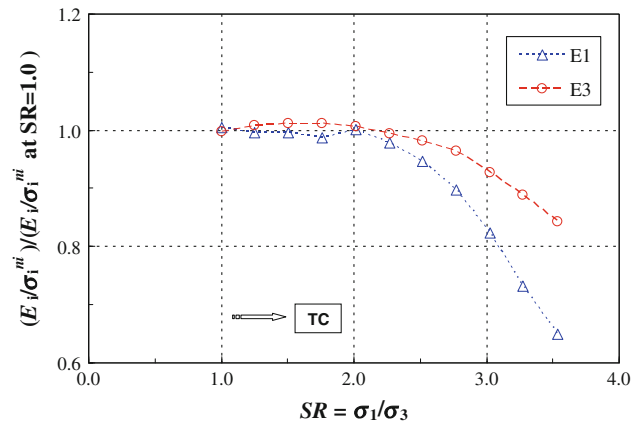

Fig. 1 Effect of stress ratio on the normalized Young's modulus (E_i/σ_i^{ni}) of Toyoura sand in different principle stress directions (data from [15])
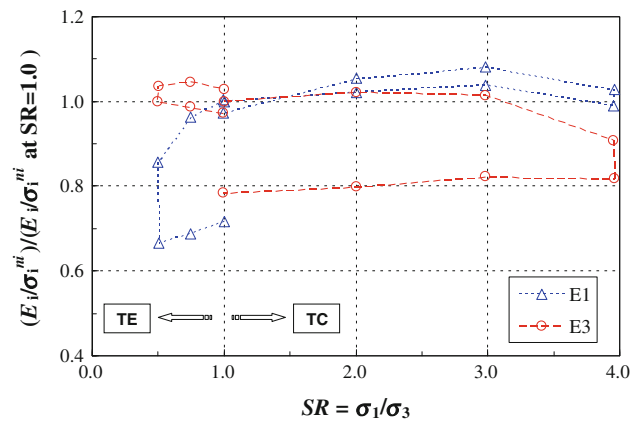

Fig. 2 Effect of stress ratio on the normalized Young's modulus (E_i/σ_i^{ni}) of Hotsun sand in different principle stress directions (data from [11])

and reported opposite results that the normalized Young's modulus in the major principle stress direction kept nearly constant, but decreased in the minor principle stress direction during TE tests or TC tests when SR was larger than SR_{th} (i.e. 3.0), as shown in Fig. 2. The results in the unloading also indicated that the damage of microstructure mainly occurred in the minor principle stress direction.

Above discussion clearly indicates that the effect of SR on the small strain stiffness is inclusive or even controversial, although the small strain stiffness has been widely used to characterize the soil properties. Hence, it is meaningful to investigate the evolution of specimen fabric during the shearing and the effect of fabric on the small strain stiffness for better understanding the fundamental mechanisms related to the soil stiffness and improving its application in characterizing soil properties.

Over the past decades, the discrete element method (DEM) has been proved to be a powerful tool for investigating the macroscopic behavior of granular materials at

Fig. 3 Schematic diagrams of sample preparation, consolidation and probe test for stiffness determination in the DEM simulation: **a** specimen before particle expansion; **b** specimen at initial state; **c** stress path in consolidation; **d** probe test for stiffness determination (not to the scale)
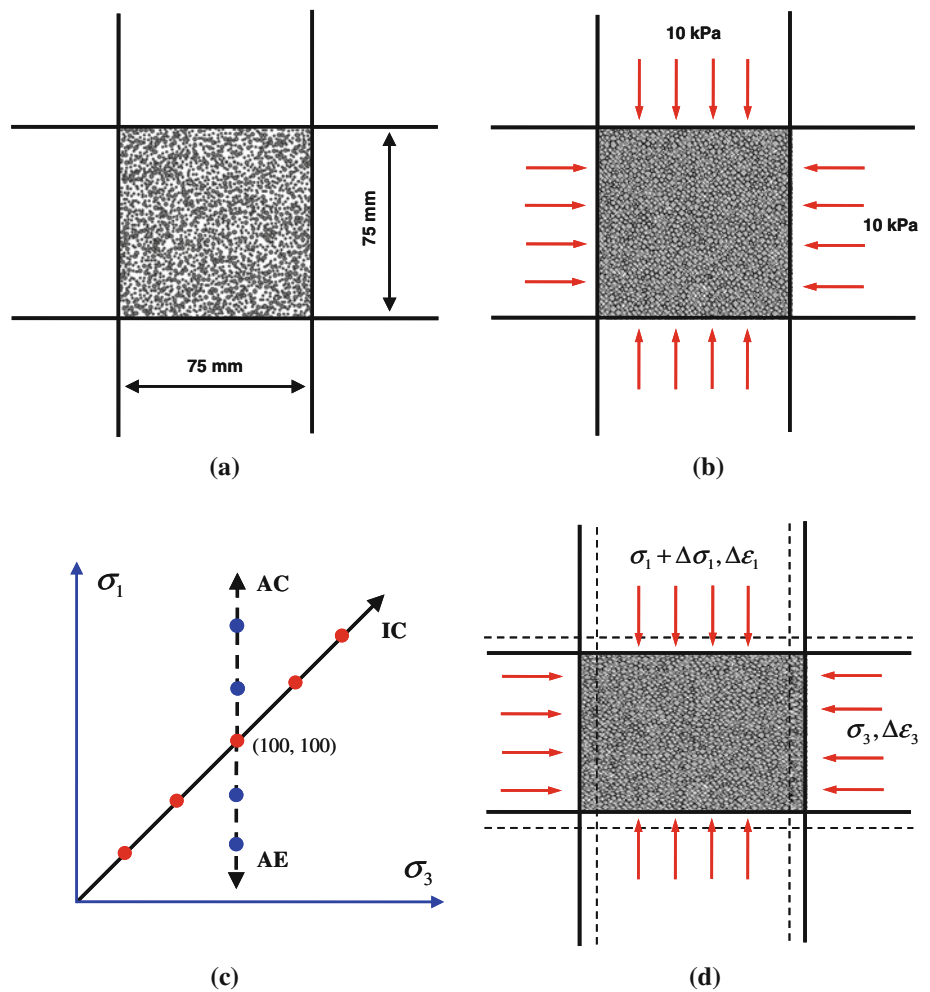
micromechanical (or particulate) level since it was proposed by Cundall and Strack [16]. Majority of the DEM simulations has been focused on the soil behavior at large strain levels (e.g. soil strength and liquefaction). Only several studies have dealt with the small strain (or elastic) properties [17–21] and how the small strain properties change with increasing stress ratio as well as the fabric of the soil has not been well investigated.

In this study, DEM simulations are carried out to evaluate the small strain stiffness of a random granular packing with focus on the effect of stress ratio. The evolutions of the small strain stiffness and the anisotropy of the packing are investigated and related to the evolution of the fabric of the packing. The influences of soil shear strength (i.e. the inter-particle friction coefficient) on the effect of *SR* and the evolution of fabric are also studied.

2 Numerical procedures

The well recognized program PFC^{2D} [22] is used to perform the DEM simulation in this study. The specimen is

Table 1 Parameters used in the simulation

Wall stiffness	Rigid	Contact law	Hertz-Mindlin
Wall-particle friction coefficient	0	Inter-particle friction coefficient	0.50
No. of particles	1878	Density	2,600 kg/m^3
Particle diameter	1.2–2.4 mm	Particle shear modulus and Poisson's ratio	29 GPa, 0.15

represented by a periodic space of 75×75 mm^2 confined with two pairs of rigid and frictionless walls (Fig. 3). The soil particles are represented by balls and their final diameters vary uniformly between 1.2 and 2.4 mm. Non-spherical particle may be adopted to represent more realistic particle shape and therefore soil behavior [23], but will not be used here to avoid excessive complexity. The effects of particle shape on the fabric and the small strain stiffness of the soil are under investigation in another study. The main parameters used in the simulation are summarized in Table 1.

Figure 3 schematically illustrates the simulation procedures, including specimen generation, isotropic and anisotropic consolidation, and perturbation test for small strain stiffness determination. First, 1878 balls with 62.5 % of their final sizes are generated randomly in the space and then expanded to their final sizes. Note that the inter-particle friction coefficient f is temporarily set to zero during the expansion. To capture the force-dependent contact stiffness and thus stress-dependent small strain stiffness, simplified Hertz-Mindlin contact law is used in this study. The detail of the used Hertz-Mindlin contact law can be found in the PFC^{2D} user manual. Then, the specimen is brought to an isotropic stress of 10 kPa by servo control of the walls. It is taken as the initial state of the specimen. The initial porosity of the specimen in this study is 0.164.

Finally, the inter-particle friction coefficient is set to 0.50 (corresponding to an inter-particle friction angle 26.6°) and the specimen can be consolidated to different stress states by servo control of the walls. In this study, the specimen is consolidated along the isotropic compression (IC) line to achieve different isotropic stress states (see Fig. 3c). To achieve anisotropic stress states, the specimen at the isotropic stress state of 100 kPa (porosity = 0.164) is consolidated along the stress path AC (axial compression) or AE (axial extension), respectively.

At each stress state, a drained biaxial test at small strain (or probe test [17]) is carried out to determine the small strain properties of the specimen, which is similar to the triaxial test by Hoque and Tatsuoka [15]. During the test, a small strain increment $\Delta\varepsilon_i$ is applied in one direction, while the stress component in the other direction σ_j is kept constant by servo control until the shear strain $\gamma_{ij} = \Delta\varepsilon_i - \Delta\varepsilon_j$ reaches 10^{-6}. As suggested by Cundall et al. [17], the inter-particle friction coefficient is temporarily set to be infinite to prevent sliding during the probe test because for small strain oscillations, contact sliding does not occur—sliding stops at the instant of unloading and sliding only resumes again at the original point of loading upon reloading. Then, the small strain Young's modulus E_i, shear modulus G_{ij} and Poisson's ratio υ_{ij} can be determined as follows:

$$
\begin{aligned}
E_i &= \frac{\Delta\sigma_i}{\Delta\varepsilon_i} \\
G_{ij} &= \frac{\Delta\tau_{ij}}{\gamma_{ij}} = \frac{\Delta\sigma_i/2}{\Delta\varepsilon_i - \Delta\varepsilon_j} \\
\upsilon_{ij} &= -\frac{\Delta\varepsilon_j}{\Delta\varepsilon_i}
\end{aligned}
\tag{2}
$$

The first number in the subscript denotes the loading direction. By changing the loading direction, the anisotropy of the specimen stiffness can be evaluated.
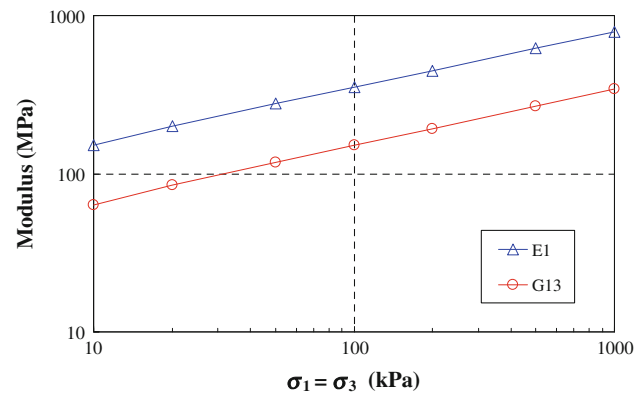
Fig. 4 Evolutions of small strain moduli E_1 and G_{13} at different isotropic stress states

3 Results and discussions

3.1 At isotropic stress states

The specimen is isotropically consolidated from 10 to 20, 50, 100, 200, 500 and 1,000 kPa and the small strain properties of the specimen are measured by the probe test at each stress state. The results indicate that the small strain properties are isotropic at these isotropic stress states (see Fig. 8) and therefore only the results of loading in the axial direction are presented here for simplicity.

Figure 4 shows the small strain Young's modulus E_1 and shear modulus G_{13} at different isotropic stress states. As seen in Fig. 4, the small strain moduli increase as the effective confining pressure increases, which indicates that the DEM simulation using Hertz-Mindlin contact law successfully predicts the stress-dependent elastic stiffness of granular soils observed in laboratory. To quantify the stress effect, the moduli are fitted by Eq. (1) and the fitted values of stress exponent n are 0.355 and 0.361 for E_1 and G_{13}, respectively. It is clear that the n values for E_1 and G_{13} are larger than 1/3 for Hertz-Mindlin contact law, which is due to the evolutions of contact number and contact force during the consolidation [24]. Moreover, the soil skeleton Poisson's ratio υ_{13} decreases as effective confining pressure increases instead of a constant that usually assumed in geotechnical analyses, as shown in Fig. 5. It is consistent with the observations in the laboratory tests [24–28].

3.2 At anisotropic stress states

Figure 6 shows the axial strain ε_1 and volumetric strain ε_v of the specimen during anisotropic consolidation along stress paths AC and AE. Note that the isotropic stress state of 100 kPa is taken as the reference state for strain calculation. As seen in Fig. 6, the stress ratio increases as the axial strain increases, but the rate of increase decreases, indicating the
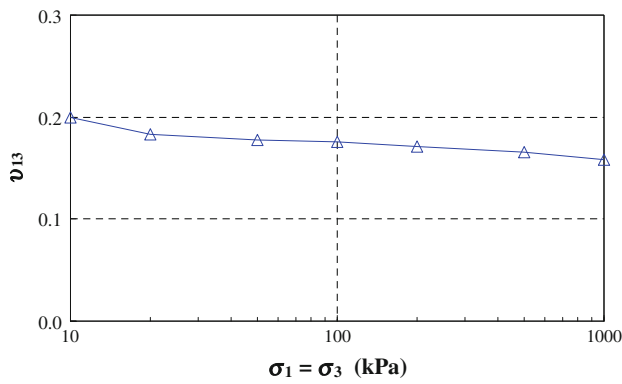
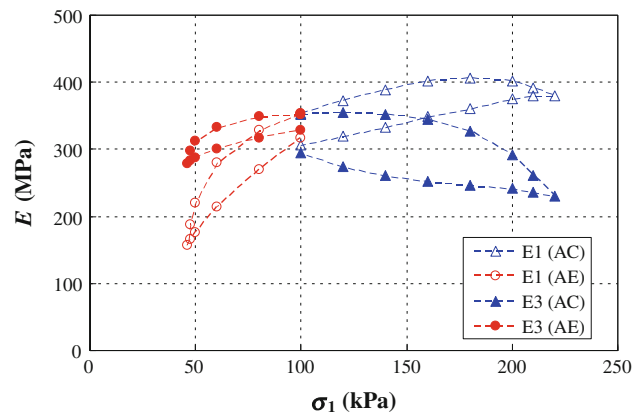**Fig. 5** Evolutions of Poisson's ratio υ_{13} at different isotropic stress states
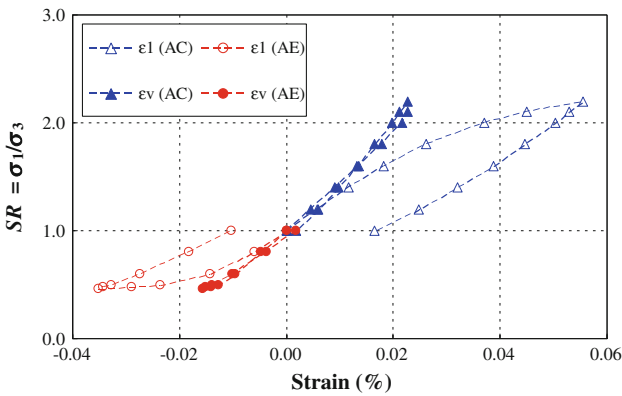
Fig. 6 Evolutions of the axial strain ε_1 and volumetric strain ε_v during anisotropic loading and unloading
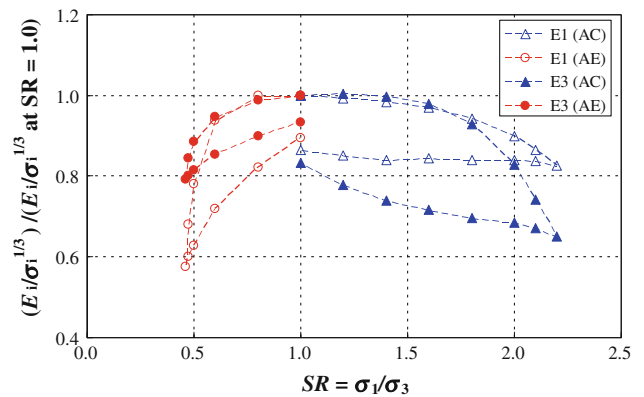

Fig. 7 Evolution of the Young's modulus with axial stress at anisotropic stress states


Fig. 8 Effect of stress ratio on the normalized Young's modulus in different principle stress directions

nonlinear soil behavior. When the specimen is unloaded to the isotropic stress state, residual axial strain exists. Regarding the volumetric strain, it behaviors almost linearly and its magnitude is rather small which means that the porosity of the specimen is nearly constant during the anisotropic consolidation in this study.

The evolutions of the Young's moduli E_1 and E_3 are plotted as a function of stress component σ_1 in Fig. 7. First, as seen in Fig. 7, the values of E_1 and E_3 are nearly the same at the initial isotropic stress state, indicating that the specimen is inherently isotropic. Second, when loaded along AC, E_1 increases as σ_1 increases first and then decreases with further increase of σ_1 (or SR). In the meantime, E_3 keeps nearly constant first and then decreases with further increase of σ_1, but the degree of decrease is more significant than that of E_1. When loaded along AE, the results show an opposite trend. Similar results are also observed in the laboratory tests by Ezaoui and Di Benedetto [11]. Such trends are expected since the Young's modulus in a given direction generally depends only on the stress component in that direction.

To better illustrate the stress ratio effect, the Young's modulus is normalized by the stress component in that direction and plotted as a function of SR in Fig. 8. It suggests that threshold stress ratio SR_{th} does exist, being around 1.60 in AC and around 0.8 in AE. The SR_{th} value in the simulation is smaller than the experimental ones (e.g. around 2.0 in [15] and 3.0 in [11]), which is probably due to the perfect rounded particle shape (i.e. no rolling resistance) and therefore low shear strength. Parametric study will be given in the following to investigate the influence of shear strength (or interparticle friction coefficient) on the SR_{th} value. When SR is less than SR_{th}, SR seems to have no effect on the normalized Young's modulus. When SR is larger than SR_{th}, the normalized Young's modulus decreases as SR increases especially in the minor principle stress direction, indicating the potential difference of fabric change in different principle stress directions. This phenomenon is consistent with the observation in Ezaoui and Di Benedetto [11] as expected, but opposite to the one in Hoque and Tatsuoka [15]. Currently, it is unknown what causes such discrepancy and further study is needed.

During the unloading process, the normalized Young's modulus in the minor principle stress direction is always smaller than that in the major principle stress direction, but
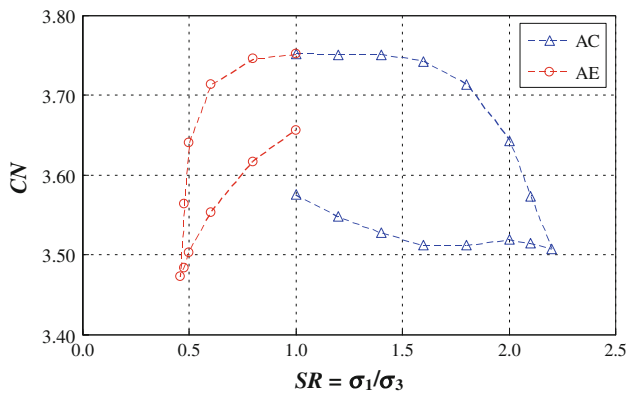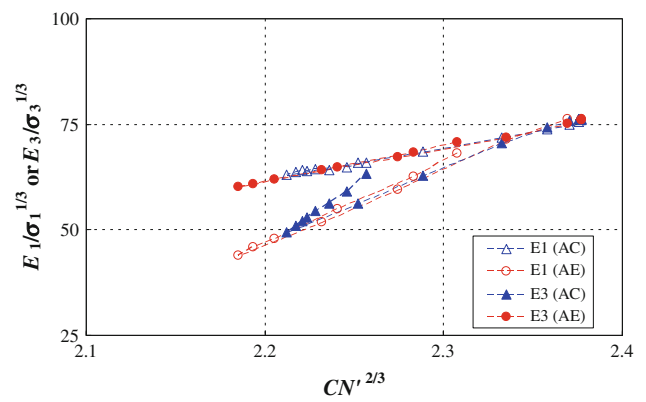
Fig. 9 Evolutions of the coordination number *CN* with stress ratio

Fig. 10 Relationship between normalized Young's modulus and modified coordination number CN' in different principle stress directions

Fig. 11 Evolutions of the ratio of Young's modulus E_1/E_3 (global anisotropy of the specimen) with stress ratio

the difference decreases as *SR* decreases. When the specimen returns to the isotropic stress state, the Young's modulus is much smaller than the one at the initial state. These important findings indicate that the microstructure of the specimen has been damaged during the shearing, especially in the minor principle stress direction, and can not be fully recovered during unloading.

Due to the particulate nature, contacts bear and transfer the loads in granular soils. Therefore, the contacts and contact forces as well as their distributions are important characteristics of an assembly at grain-scale level. It is thus meaningful to examine their evolutions during the loading and unloading processes. Figure 9 shows the evolution of coordination number *CN*, which means the average number of contacts per particle. Note that here only the particles with more than two contacts are taken into account to calculate the total contact number, while all the particles are used to evaluate the porosity [29]. As seen in Fig. 9, the value of *CN* remains nearly constant when *SR* is less than SR_{th}. With further increase of *SR*, *CN* decreases significantly and cannot be fully recovered during unloading. By comparing Figs. 8 and 9, it is of great interest to find that the shape of the evolution of normalized Young's modulus is almost the same as the evolution of *CN*. Gu [24] shows that at isotropic stress states, the small strain stiffness of granular soils is linearly proportional to $(CN')^{2/3}$, where CN' is the modified coordination number which accounts for the nonuniform distribution of normal contact forces. In calculating CN', each contact is multiplied by a stiffness factor given by $(F_i/F_{avg})^{1/3}$, where F_i is the i-th normal contact force and F_{avg} is the average normal contact force. Figure 10 shows the relationship between the normalized Young's modulus and the value of $(CN')^{2/3}$. As seen in Fig. 10, the normalized Young's modulus is closely related to microscopic *CN*, although difference exists in the major principle stress and minor principle stress directions. This is due to the anisotropic distribution of contact number in the specimen at anisotropic stress state as illustrated
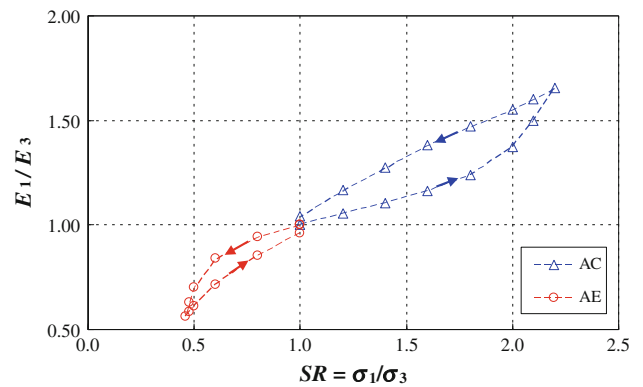
below, but *CN* only describes the overall contact number of the specimen.

The ratio of directional Young's modulus E_1/E_3 is usually adopted as an index of the global anisotropy of the specimen [11,15,30,31]. Figure 11 shows the evolution of E_1/E_3 as a function of *SR*. At initial stress state ($SR = 1.0$), the value of E_1/E_3 is unit, indicating the specimen is inherently isotropic or the inherent anisotropy is negligible. Therefore, any anisotropy of the specimen will be the induced anisotropy by the shearing process. For easy explanation, here the induced anisotropy is conceptually divided into two parts: anisotropy of contact numbers (i.e. fabric anisotropy) and anisotropy of contact forces. As seen in Fig. 11, the anisotropy of the specimen increases smoothly as *SR* increases when *SR* is less than SR_{th}, but significantly when *SR* is larger than SR_{th}. Keeping in mind the evolution of *CN*, it can be deduced that the anisotropy mainly results from the anisotropy of contact forces when *SR* is less than SR_{th}. Meanwhile, the degree of anisotropy is higher during unloading than that during loading at the same *SR* value,
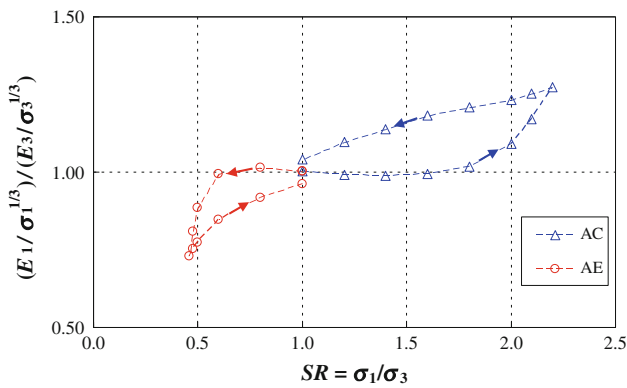
Fig. 12 Evolutions of the ratio of normalized Young's modulus $(E_1/\sigma_1^{1/3})/(E_3/\sigma_3^{1/3})$ (fabric anisotropy of the specimen) with stress ratio

indicating that the induced fabric anisotropy may be reserved during unloading.

To allow a better illustration of the fabric anisotropy, a new macroscopic anisotropy index $(E_1/\sigma_1^{1/3})/(E_3/\sigma_3^{1/3})$ is proposed and its evolution with SR is shown in Fig. 12. It is clear that fabric anisotropy is not induced when SR is less than SR_{th}, indicating that only the contact forces are adjusted to resist the external loads. When SR increases to being larger than SR_{th}, the specimen has to adjust not only the contact forces, but also the fabric to resist the external loads.

Taking advantages of the numerical simulation, the evolution of the micro information of the specimen during shearing is analyzed to study the macroscopic anisotropy of the specimen at microscopic level. The results indicate that the evolutions of the micro information in AC and AE are quite similar and therefore here only the results in AC are presented for simplicity. Figure 13 shows the rose diagrams of the distributions of contact number and normal contact force (NCF)

during loading along AC. As seen in Fig. 13a, the contact number remains nearly constant when SR is less than SR_{th}, and then decreases significantly in the horizontal direction and slightly in the vertical direction when SR is larger than SR_{th}. It indicates that the damage of the fabric mainly occurs in the minor principle stress direction, which reasonably explains the different evolutions of Young's modulus in different directions. On the other hand, the NCF increases significantly in the vertical direction and remains nearly the same in the horizontal direction, which results from the loading mode.

Figure 14 shows the rose diagrams of the distributions of contact number and normal contact force during unloading along AC. It offers several important findings: first, the contact number may decrease in the vertical direction during unloading, although SR decreases; second, the contact number in the horizontal direction recovers slowly when SR is larger than SR_{th}, and then recovers quickly with further decrease of SR. It means that the specimen also adjusts the contact forces first and then additional fabric to resist external loads during unloading; third, when the specimen is unloaded to the isotropic stress state, anisotropy with a slightly higher stiffness in the major principle stress direction is induced by the historical shearing process. It should be emphasized that the damage of the fabric is significant, indicated by the reduction of CN and the macroscopic Young's modulus.

To link the microscopic fabric anisotropy and the macroscopic anisotropy indicated by the ratio of normalized Young's modulus $(E_1/\sigma_1^{1/3})/(E_3/\sigma_3^{1/3})$, the density function of the distributions of the contact orientations $R(\theta)$ proposed by Rothenburg and Bathurst [32] is used here to quantify the fabric anisotropy:
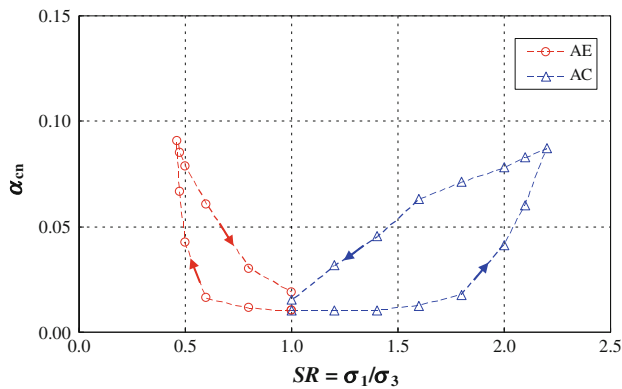
$$R(\theta) = \frac{1}{2\pi} \{1 + \alpha_{\text{cn}} \cos 2(\theta - \theta_{\text{cn}})\} \qquad (3)$$
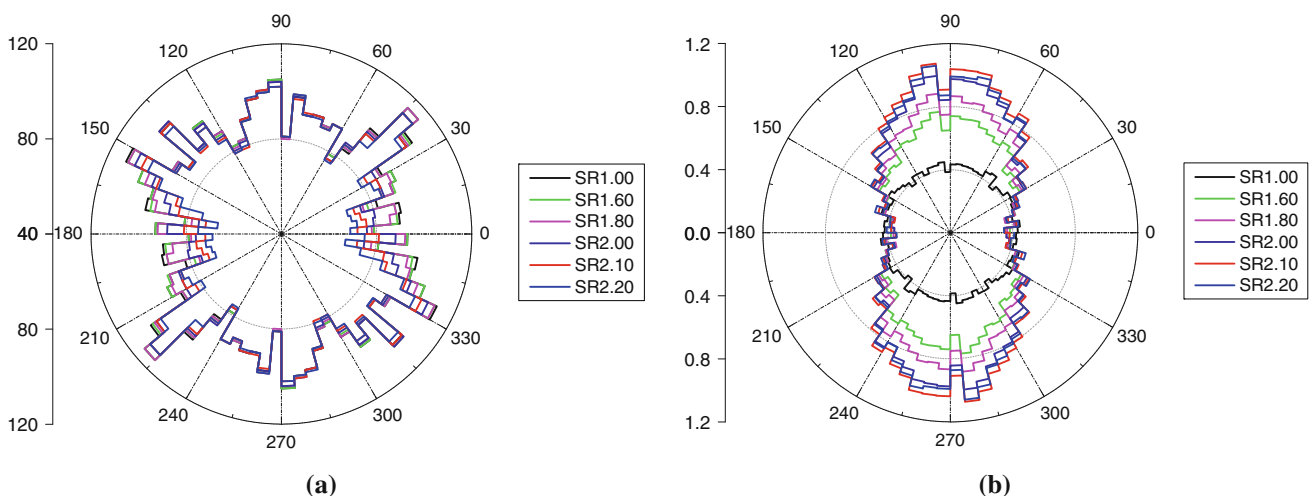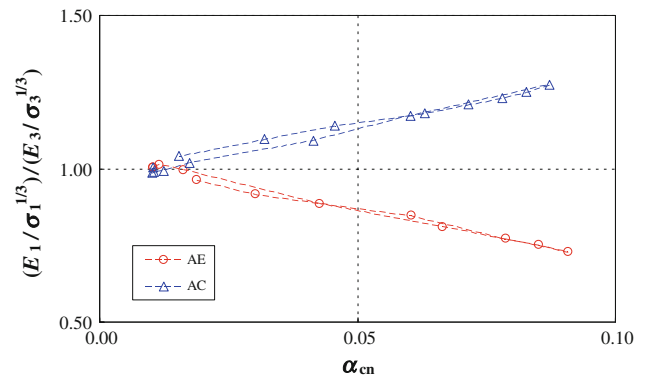

Fig. 13 Evolutions of the micro information in AC loading: angular distributions of **a** contact number; **b** normal contact force (N)
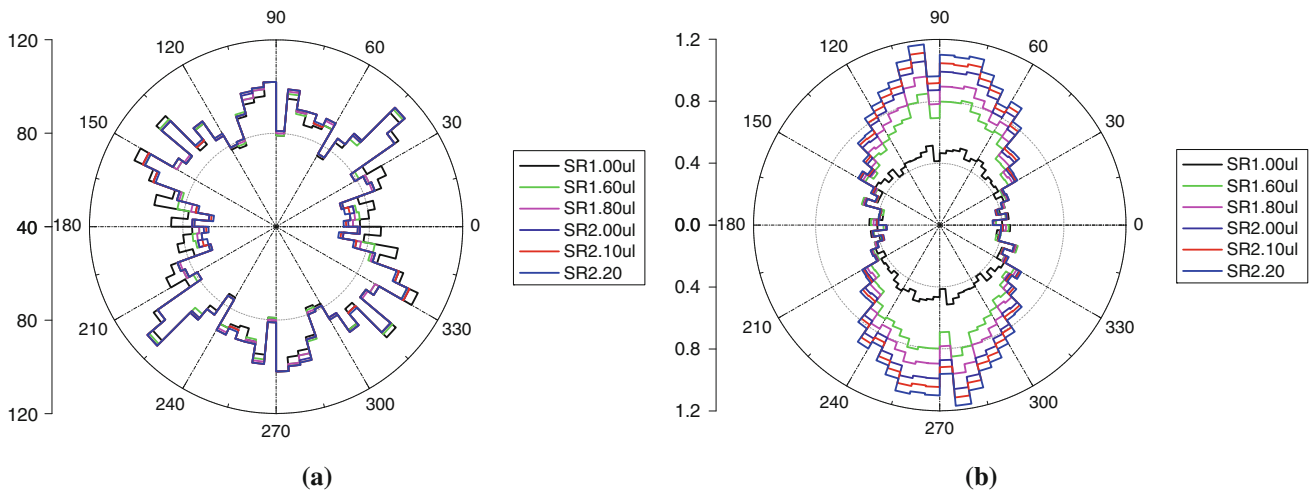
Fig. 14 Evolutions of the micro information in AC unloading: angular distributions of **a** contact number; **b** normal contact force (N)

Fig. 15 Evolution of the fabric anisotropy factor α_{cn} with stress ratio
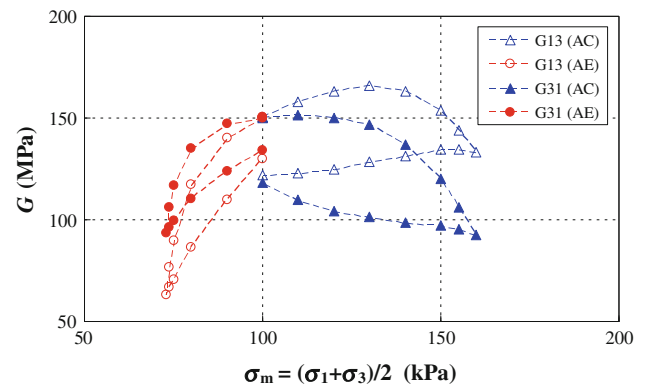

Fig. 16 Relationship between the ratio of normalized Young's modulus $(E_1/\sigma_1^{1/3})/(E_3/\sigma_3^{1/3})$ and fabric anisotropy factor α_{cn}

Fig. 17 Evolution of small strain shear modulus with mean effective stress

where α_{cn} is a factor defining the magnitude of the anisotropy, θ defines the contact orientation, and θ_{cn} defines the principle direction of the anisotropy.

Figure 15 shows the evolution of fabric anisotropy factor α_{cn} with the stress ratio. It suggests that α_{cn} remains nearly the constant when SR is less than SR_{th}. When SR is larger than SR_{th}, α_{cn} increases significantly, together with the reduction of contact number (Fig. 9). During unloading, α_{cn} is much larger than that during loading at the same SR value, indicating fabric anisotropy is induced by the historical shearing process. Figure 16 shows the relationship between the ratio of normalized Young's modulus $(E_1/\sigma_1^{1/3})/(E_3/\sigma_3^{1/3})$ and fabric anisotropy factor α_{cn}. It is interesting that the value of $(E_1/\sigma_1^{1/3})/(E_3/\sigma_3^{1/3})$ is linearly proportional to the value of α_{cn}, indicating $(E_1/\sigma_1^{1/3})/(E_3/\sigma_3^{1/3})$ can be served as an indicator of the fabric anisotropy.
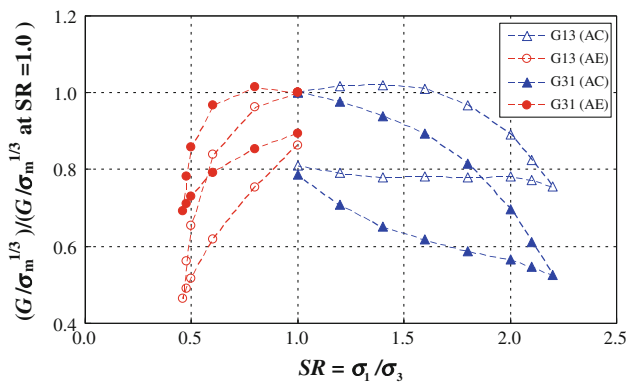
As suggested by Yu and Richart [9], the small strain shear moduli G_{13} and G_{31} at anisotropic stress states are plotted against the mean effective stress $\sigma_m = (\sigma_1 + \sigma_3)/2$ in Fig. 17. It shows that the shear modulus corresponding to the loading

in the major principle stress direction is always higher than the other one, which is against the common assumption that they are equal to each other. In laboratory, G_{13} is usually measured by the shear wave of propagation in the axial direction and particles moving in the radial direction, while G_{31} by the
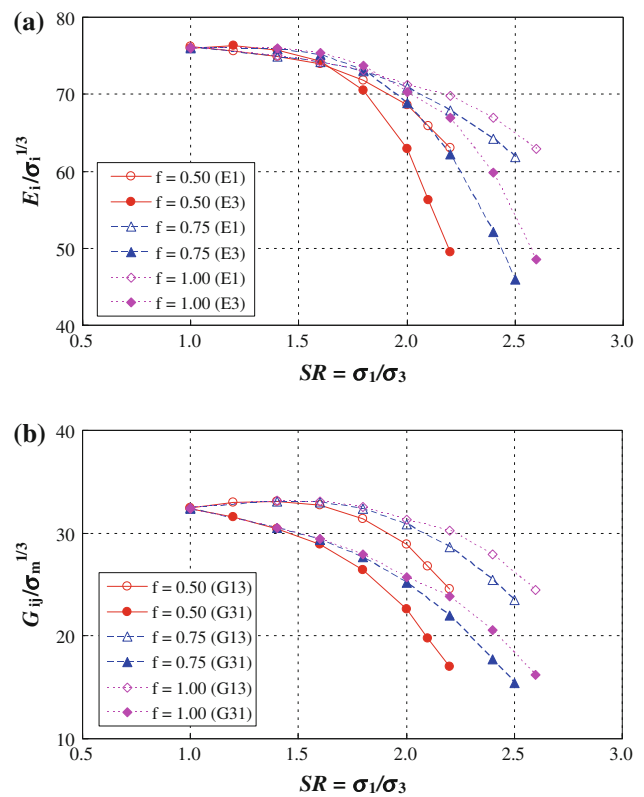
Fig. 18 Effect of stress ratio on the normalized small strain shear modulus

Fig. 19 Influence of the inter-particle friction coefficient on the effect of stress ratio: **a** Young's modulus; **b** shear modulus (modulus in MPa, stress in kPa)

shear wave of propagation in the radial direction and particles moving in the axial direction. Kuwano and Jardine [14] reported similar result and explained that it resulted from the preferred wave path along the strong force chain in the major principle stress direction. This explanation is supported by the distribution of normal contact forces in the specimen at anisotropic stress states (Fig. 13).

It also can be seen in Fig. 17 that the shear modulus during unloading is much smaller than the one during loading at the same stress condition, which is similar to the test results in Yu and Richart [9]. It indicates the microstructure is damaged by the historical shearing process. To better illustrate the SR effect, the normalized shear modulus $G/\sigma_m^{1/3}$ is divided by the one at $SR = 1.0$ and plotted as a function of SR in Fig. 18. For G_{13}, it keeps nearly constant when SR is less than SR_{th} and then starts to decrease with further increase of SR in AC. However, it always decreases with increasing SR in AE and the degree of decrease is more significant than that in AC. These observations are the same as the one in the laboratory tests by Tatsuoka et al. [6]. G_{31} shows similar trends as G_{13} when the change of major principle stress direction is concerned. Similar to the Young's modulus, the evolution of shear modulus results from the evolution of fabric.

3.3 Effect of soil shear strength

It seems that the SR_{th} value in the simulation is somewhat smaller than that in the laboratory test, which is probably due to the perfect rounded particle shape (i.e. no rolling resistance) and therefore low shear strength. It is consistent with the results by Yu and Richart [9] that the effect of SR depends on the shear strength. Generally, particle with certain aspect ratio (non-spherical particle) or high inter-particle friction coefficient can be used to increase the soil shear strength [33–36]. To avoid excessive completeness, only the inter-particle friction coefficient is increased to increase the soil shear strength. Additional two inter-particle friction

coefficients (i.e. 0.75 and 1.00) are used to investigate its influence on the effect of SR and the evolution of fabric. The analyses find that the maximum available stress ratios SR_{max} are 2.36, 2.72 and 2.98 for the specimens with f values of 0.50, 0.75 and 1.00, corresponding to macroscopic friction angles of 23.9°, 27.5° and 29.8° respectively.

Figure 19 shows the effect of SR on the small strain stiffness at different f values during loading in AC. It is clear that the effect of SR on the small strain stiffness becomes less significant as f increases, which agrees well with the results in Ng and Petrakis [19]. Keeping in mind the relation between small strain stiffness and CN, the influence of f on the evolution of CN is shown in Fig. 20. As expected, CN decreases slowly with increasing SR as f increases, which is consistent with the evolution of small strain stiffness.

The influence of f on the ratio of normalized Young's modulus $(E_1/\sigma_1^{1/3})/(E_3/\sigma_3^{1/3})$ and fabric anisotropy factor α_{cn} is shown in Fig. 21. As seen in Fig. 21, higher SR is needed to induce fabric anisotropy as f increases, which means that SR_{th} increases with increasing f value or shear strength. As suggested by Yu and Richart [9], a normalized stress ratio factor $k_{SR} = (SR - 1)/(SR_{max} - 1)$ is used to reflect the influence of soil strength on the effect of SR. Figure 22 shows the variations of the coordination number
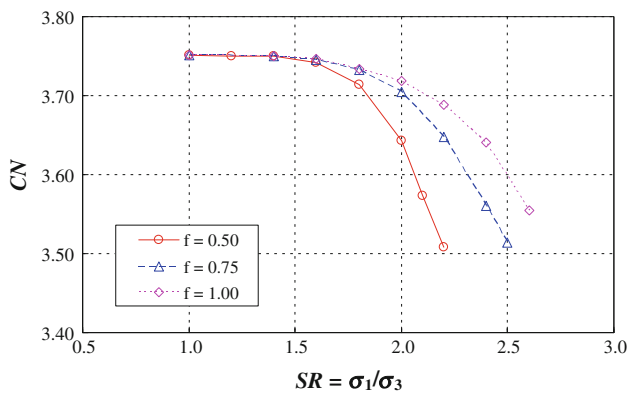
Fig. 20 Influence of the inter-particle friction coefficient on the evolution of coordination number with stress ratio
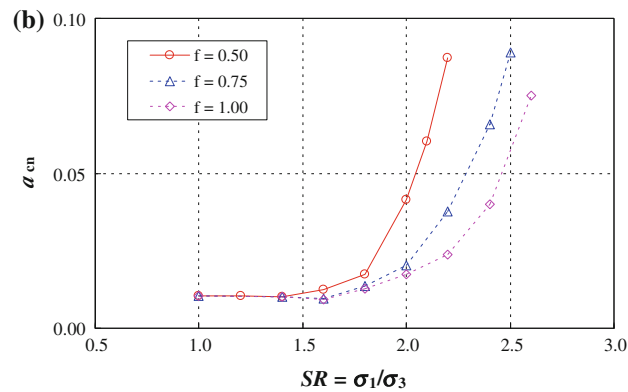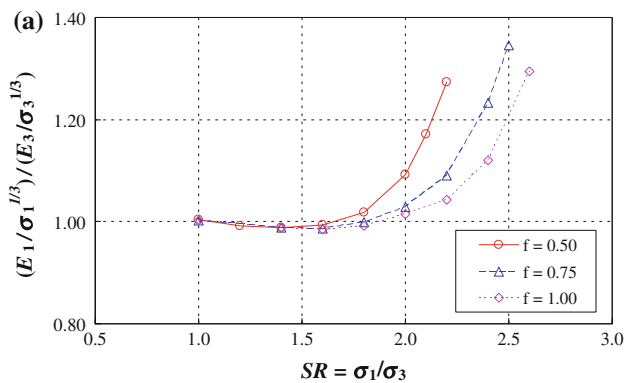
Fig. 21 Influence of the inter-particle friction coefficient on the evolutions of **a** normalized Young's modulus $(E_1/\sigma_1^{1/3})/(E_3/\sigma_3^{1/3})$ and **b** fabric anisotropy factor

CN and fabric anisotropy factor α_{cn} with k_{SR}. It is interesting to observe that the relationships become unique when the differences of soil shear strength are considered. Therefore, the lower SR_{th} value in the simulation than that in the laboratory test can be convincingly explained as the lower shear strength in the simulation due primarily to the perfect rounded particle shape. Meanwhile, numerical studies of the particle shape effect on the small strain stiffness and soil fabric are undergoing.
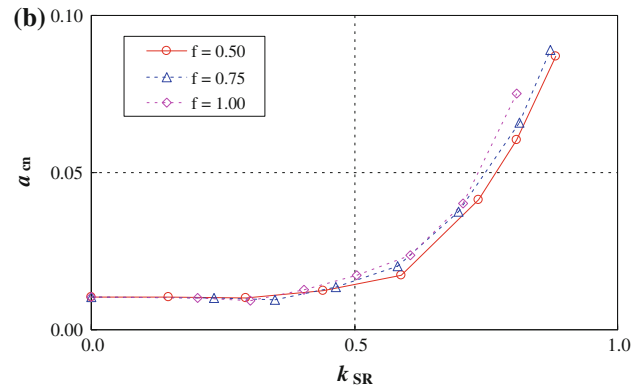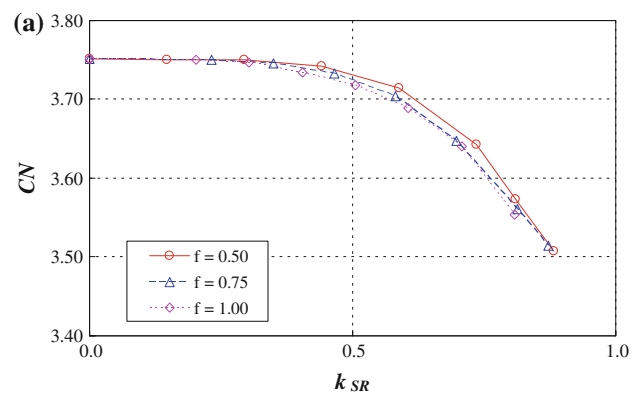
Fig. 22 Evolutions of **a** coordination number CN and **b** fabric anisotropy factor α_{cn} with normalized stress ratio factor k_{SR}

4 Summary and conclusions

This study performed DEM simulations to evaluate the small strain stiffness of a granular random packing with focus on the effect of stress ratio. The evolutions of the small strain stiffness as well as the anisotropy of the packing were investigated and related to the evolution of the micro information of the packing. The main findings of this study can be summarized as follows:

(a) At isotropic stress states, the small strain Young's modulus and shear modulus increase with increasing mean effective stress, indicating that the DEM simulation with Hertz-Mindlin contact law can successfully capture the stress-dependent characteristic of the small strain stiffness. Meanwhile, Poisson's ratio decreases with mean effective stress instead of a constant, which is consistent with the experimental results.

(b) At anisotropic stress states, there is a threshold stress ratio SR_{th}, which characterizes the fabric change during the shearing. When SR is less than SR_{th}, the contact number remains nearly constant and only the contact forces adjust to resist the external load. The anisotropy of the specimen stiffness mainly results from the anisotropy of

contact forces. When SR is larger than SR_{th}, however, the contact number decreases significantly in the minor principle stress direction and slightly in the major principle stress direction besides the adjustment of contact forces. The anisotropy of the specimen stiffness results from the anisotropies of fabric and contact forces. During unloading, only partial contacts recover, indicating the damage of fabric due to the historical shearing process. It is also found that the SR_{th} value increases with the shear strength (or inter-particle friction coefficient) of the granular soil.

(c) The Young's modulus in a given direction generally depends on the stress component in that direction when SR is less than SR_{th}. After that, the Young's modulus decreases due primarily to the decrease of contact number by the shearing, particularly in the minor principle stress direction. The results also show that the evolution of Young's modulus is closely related to the evolution of coordination number.

(d) The macroscopic anisotropy of small strain stiffness results from the anisotropy of the micro information (i.e. the distribution of contact force and contact number). Generally, the ratio of E_1/E_3 describes the global anisotropy of the specimen, while $E_1/\sigma_1^{1/3}/(E_3/\sigma_3^{1/3})$ reflects the fabric anisotropy.

(e) Regarding the shear moduli G_{13} and G_{31}, they are not equal to each other, and this is not congruous to the common assumption in soil mechanics. The reason lies in the particulate nature of granular material and the anisotropy of specimen at anisotropic stress states.

References

1. Richart, F.E., Hall, J.R., Woods, R.D.: Vibrations of Soils and Foundations. Prentice-Hall, Englewood Cliffs (1970)
2. Andrus, R.D., Stokoe, K.H.I.I.: Liquefaction resistance of soils from shear-wave velocity. J. Geotech. Geoenviron. Eng. **126**(1), 1015–1025 (2000)
3. Yang, J., Yan, X.R.: Site response to multi-directional earthquake loading: a practical procedure. Soil Dyn. Earthq. Eng. **29**(4), 710–721 (2000)
4. Hardin, B.O., Richart, F.E.: Elastic wave velocities in granular soils. J. Soil Mech. Found. Div. **89**(SM1), 39–56 (1963)
5. Hardin, B.O., Black, W.L.: Sand stiffness under various triaxial stresses. J. Soil Mech. Found. Div. **92**(2), 27–42 (1966)
6. Tatsuoka, F., Iwasaki, T., Fukushima, S., Sudo, H.: Stress conditions and stress histories affecting shear modulus and damping of sand under cyclic loading. Soils Found. **19**(2), 29–43 (1979)
7. Roesler, S.K.: Anisotropic shear modulus due to stress anisotropy. J. Geotech. Eng. Div. **105**(7), 871–880 (1979)
8. Knox, D.P., Stokoe, K.H.II., Kopperman, S.E.: Effect of state of stress on velocity of low-amplitude shear wave propagation along principle stress directions in dry sand. Geotechnical Engineering report GR-82-23, University of Texas at Austin, Texas (1982)
9. Yu, P.-J., Richart Jr, F.E.: Stress ratio effects on the shear modulus of dry sands. J. Geotech. Eng. Div. **110**(3), 331–345 (1984)
10. Chen, Y.-C., Ishibashi, I., Jenkins, J.T.: Dynamic shear modulus and fabric: part I, depositional and induced anisotropy. Géotechnique **38**(1), 25–32 (1988)
11. Ezaoui, A., Di Benedetto, H.: Experimental measurements of the global anisotropic elastic behavior of dry Hostun sand during triaxial tests, and the effect of sample preparation. Géotechnique **59**(7), 621–635 (2009)
12. Bellotti, R., Jamiolkowski, M., Lo Presti, D.C.F., O'Neill, D.A.: Anisotropy of small strain stiffness in Ticino sand. Géotechnique **46**(1), 115–131 (1996)
13. Hoque, E., Tatsuoka, F.: Anisotropy in elastic deformation of granular materials. Soils Found. **38**(11), 163–179 (1998)
14. Kuwano, R., Jardine, R.J.: On the applicability of cross-anisotropic elasticity to granular materials at very small strains. Géotechnique **52**(10), 727–749 (2002)
15. Hoque, E., Tatsuoka, F.: Effects of stress ratio on small-strain stiffness during triaxial shearing. Géotechnique **54**(7), 429–439 (2004)
16. Cundall, P.A., Strack, O.D.L.: A discrete numerical model for granular assemblies. Géotechnique **29**(1), 47–65 (1979)
17. Cundall, P.A., Jenkins, J.T., Ishibashi, I.: Evolution of elastic moduli in a deforming granular assembly. In: Biarez, J., Gourves, R. (eds.) Powders and Grains, pp. 319–322. Balkema, Rotterdam (1989)
18. Dobry, R., Ng, T.T.: Discrete modeling of stress-strain behavior of granular media at small and large strains. Eng. Comput. **9**, 129–143 (1992)
19. Ng, T.T., Petrakis, E.: Small-strain response of random array of spheres using discrete element method. J. Eng. Mech. **122**(10), 239–244 (1996)
20. Magnanimo, V., La Ragione, L., Jenkins, J.T., Wang, P., Makse, H.A.: Characterizing the shear and bulk moduli of an idealized granular material. Europhys. Lett. **81**(3), 34006 (2008)
21. Wang, Y.H., Mok, C.M.B.: Mechanisms of small-strain shear-modulus anisotropy in soils. J. Geotech. Geoenviron. Eng. **134**(10), 1516–1530 (2008)
22. Itasca: Particle flow code (PFC^{2D}) manual, Itasca Consulting Group, Inc., Minn. (2003)
23. O'Sullivan, C., Bray, J.D., Riemer, M.F.: Influence of particle shape and surface friction variability on response of rod-shaped particulate media. J. Eng. Mech. **128**(11), 1182–1192 (2002)
24. Gu, X.Q.: Dynamic properties of granular materials at the macro and micro scales. PhD thesis, The University of Hong Kong, Hong Kong (2012)
25. Kokusho, T.: Cyclic triaxial test of dynamic soil properties for wide strain range. Soils Found. **20**(2), 45–60 (1980)
26. Nakagawa, K., Soga, K., Mitchell, J.K.: Observation of Biot compressional wave of the second kind in granular soils. Géotechnique **47**(1), 133–147 (1997)
27. Wichtmann, T., Triantafyllidis, T.: On the influence of the grain size distribution curve on P-wave velocity, constrained elastic modulus M_{max} and Poisson's ratio of quartz sands. Soil Dyn. Earthq. Eng. **30**, 757–766 (2010)
28. Kumar, J., Madhusudhan, B.N.: Effect of relative density and confining pressure on Poisson ratio from bender-extender element tests. Géotechnique **60**(7), 561–567 (2010)
29. Thornton, C.: Numerical simulations of deviatoric shear deformation of granular media. Géotechnique **50**(1), 43–53 (2000)

30. Jiang, G.-L., Tatsuoka, F., Flora, A., Koseki, J.: Inherent and stress-state-induced anisotropy in very small strain stiffness of a sandy gravel. Géotechnique **47**(3), 509–521 (1997)

31. Ishibashi, I., Caper, O.F.: Anisotropy and its relation to liquefaction resistance of granular material. Soils Found. **43**(5), 149–159 (2003)

32. Rothenburg, L., Bathurst, R.J.: Analytical study of induced anisotropy in idealized granular materials. Géotechnique **39**(4), 601–614 (1989)

33. Lu, Y., Frost, J.D.: Three-dimensional DEM modeling of triaxial compression of sands. In: Meier, R., Abbo, A., Wang, L.B. (eds.) GeoShanghai 2010 International Conference, ASCE, pp. 220–226 (2010)

34. Yan, W.M.: Particle elongation and deposition effect to macroscopic and microscopic responses of numerical direct shear tests. Geotech. Test. J. **34**(3), 238–249 (2011)

35. Barreto, D., O'Sullivan, C.: The influence of interparticle friction and the intermediate stress ratio on soil response under generalized stress conditions. Granul. Matter **14**(4), 505–521 (2010)

36. Yimsiri, S., Soga, K.: DEM analysis of soil fabric effects on behavior of sand. Géotechnique **60**(6), 483–495 (2010)